Long-Range One-Dimensional Longitudinal Optical Binding

V. Karásek, T. Čižmár, O. Brzobohatý, and P. Zemánek*

*Institute of Scientific Instruments of the ASCR, v.v.i., Academy of Sciences of the Czech Republic,
Kralovopolska 147, 612 64 Brno, Czech Republic*

V. Garcés-Chávez and K. Dholakia

SUPA, School of Physics and Astronomy, University of St. Andrews, North Haugh, Fife, KY16 9SS, United Kingdom

We create extended longitudinally optically bound chains of microparticles with the use of counter-propagating "nondiffracting" light fields, the so-called Bessel beams. The beam homogeneity and extended propagation range allow the creation of 200 μm long chains of organized microparticles. We observe short-range multistability within a single chain and long-range multistability between several distinct chains. Our observations are supported by theoretical results of the coupled dipole method.

Introduction.—Optical binding [1] denotes an interesting type of light-matter interaction for microscopic objects which leads to self-arrangement into so-called "optical matter" [2]. This intriguing self-arrangement is based upon the delicate equilibrium between the optical forces resulting both from the incident beam and from the light rescattered by the objects which then results in well-defined stable equilibrium positions for the particles concerned. The mechanism is different from the well-known optical trapping because here no predefined potential energy wells (optical traps) exist before the objects are placed into the field. The presence of the objects modifies the field distribution so that possible optical traps are created for interacting objects. The optical binding may pave the way for controlled self-assembly of colloidal particles solely by light.

In this Letter we concentrate on longitudinal optical binding [3,4] occurring along the beam propagation while laterally the objects are confined by the gradient force to the high intensity core of the beam. In contrast to the lateral (transverse) binding [1] the longitudinal binding forms optical matter in three dimensions far from any surface and has the potential for long-range particle arrangement. We demonstrate long-range 1D optical binding of particles placed within propagation invariant (nondiffracting) Bessel light beams in a counterpropagating (CP) geometry. The optical forces corresponding to light scattering by the objects are dominant over gradient forces because the Bessel beam (BB) has negligible intensity variation along its propagation axis. The beam is not significantly disturbed by the inserted objects due to its self-reconstructing property [5–7]. Using the experimental configuration [8] we have observed the first signatures of multistability within a bound matter system. We have also explored the dynamics of each particle in a self-arranged single chain (with various numbers of particles) and of bound systems with two or three such chains. The determination of the particles' equilibrium positions and phase transitions of the system (when additional particles cause the bound structure to become unstable and collapse) is supported by numerical modeling.

Theoretical background.—To interpret our experimental data we developed a numerical model based upon the coupled dipole method (CDM) [10–13]. This method is based on dividing each object into elementary, mutually interacting dipoles placed on an orthogonal grid with interdipole distances so small that the field in the vicinity of each dipole can be considered uniform. In our case we use the criterion that the distance between the dipoles is smaller than $\lambda/40$ (λ is the illuminating wavelength in the medium). The CDM calculates the distribution of dipole moments of individual dipoles modelling the objects. The total force acting upon each object is then obtained as the sum of forces acting upon these dipoles [14]. The total forces are calculated for various interparticle separations (IPS) and stable configurations are determined [13] by analysis of forces from all possible IPS.

An example of the total force acting on particle *R*, which is one of the two particles placed on the optical axis of two coaxial CP incoherent BBs, is shown in Fig. 1. In this symmetrical configuration this force is identical to so-called binding force between both objects. We interpret a negative force as resulting in a mutual attraction while a positive force is repulsive and separates the particles. Two force modulations are visible—with long and short spatial periods. Their origin is clarified in Fig. 2 and is based upon the interference of the incident BB and far-field scattered spherical waves. Since the typical IPS is much longer than the laser wavelength, the interaction between particles due to the scattered near field is neglected in this qualitative description but is considered in the quantitative CDM calculations. The overall shape of the force curve reveals a long-period modulation (henceforth termed "waves") which originates from the interference of one incident BB with its scattered field propagating in the same direction as the incident BB. This interference of copropagating
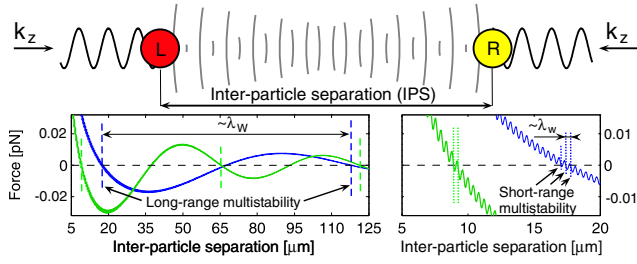
FIG. 1 (color online).   CDM calculated optical force acting upon the right-hand side particle R in a two-particle setup (*upper scheme*). *Left* plot shows overall shape of the force revealing waves related to the long-range multistability denoted by vertical dashed lines separated by about λ_W. Wavelets are apparent in the detailed view in the *right* plot and cause short-range multistability marked by vertical dotted lines separated by about λ_w. Polystyrene spheres of diameter 802 nm are placed in two counterpropagating incoherent identical Bessel beams with core radii ρ_0 (calculated for two values of ρ_0: 1.787 μm—green thick, 2.380 μm—blue thin). The following parameters were used for the CDM calculation: refractive index of particles $n_p = 1.5755 + 0.0006i$ and surrounding medium D_2O $n_m = 1.320$; laser wavelength in vacuum 1070 nm. The on-axis optical intensity of one beam 3.86 mW/μm^2 corresponded well to the experimental value [8].

waves is a result of different wave vectors of incident and scattered field along the optical axis. The BB propagates as a conical intersection of plane waves with the axial component of the wave vector $k_z = k \cos\alpha_0$, where k is the wave vector length in the medium surrounding the particles and α_0 is the polar angle of the plane waves forming the BB [9]. However, the field scattered by a particle propagates with wave number equal to k. Therefore, the part of the total force acting on particle R resulting from this mechanism is modulated with a period
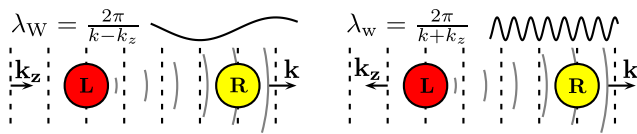

FIG. 2 (color online).   Two principal mechanisms responsible for short- and long-range multistability. The force influencing particle R due to the light scattering from particle L depends on the propagation direction of the incoming Bessel beam (BB). The dashed vertical lines show the wave fronts of the incoming Bessel beam with the axial component of the wave vector k_z and the full curves denote parts of the scattered spherical wave fronts of wave vector k on the axis. *Left scheme*. The BB comes from the left and propagates in the same direction as scattered field from particle L. The interference of copropagating fields causes force modulation driven by a long period λ_W (so-called waves). *Right scheme*. The BB comes from the right and counterpropagates with respect to the field scattered from particle L. Therefore a short-period force modulation λ_w exists (wavelets). If both particles are illuminated by two counterpropagating incoherent BBs, both mechanisms determine the total force acting on particle R as well as on particle L.

close to $\lambda_W = 2\pi/(k - k_z) = \lambda/(1 - \cos\alpha_0)$. The short-period modulations (henceforth termed "wavelets") are caused by the interference of one incident BB with its scattered field propagating in the opposite direction as the incident BB. In this case, the period of the total force modulation is close to $\lambda_w = 2\pi/(k + k_z) = \lambda/(1 + \cos\alpha_0)$. In the setup of two CP (mutually noninterfering) BBs both mechanisms combine. The waves dictate the overall shape of the total force while the wavelets create multistability and both result in numerous stable configurations of two particles with different IPS—*short-range* and *long-range* multistability. In the real situation the number of particles, their properties, and also more complex scattered-field interactions between particles influence their IPS and both types of multistabilities (their periodicities were estimated above as λ_w and λ_W).

Short-range multistability of two particles.—It has been already reported experimentally and theoretically that there exists a series of bound states (particles multistability) for *lateral* binding configuration for different properties of bound objects [1,15–17]. Here the distance between neighboring equilibrium positions of the particles in a stable chain of two particles is close to λ. In the case of *longitudinal* binding, bistable behavior has been reported [18,19]. Multistability has been predicted theoretically [13] and this paper provides the first experimental verification of this prediction (see the stairlike curves in Fig. 3).

Previous theoretical studies [13,20] have revealed a strong dependence of the number of multistable configurations upon the objects sizes and the BB core radii. Here we choose two diameters of the polystyrene spheres (802 and 1070 nm) which should behave differently with respect to the multistable configurations. Figure 3 compares the
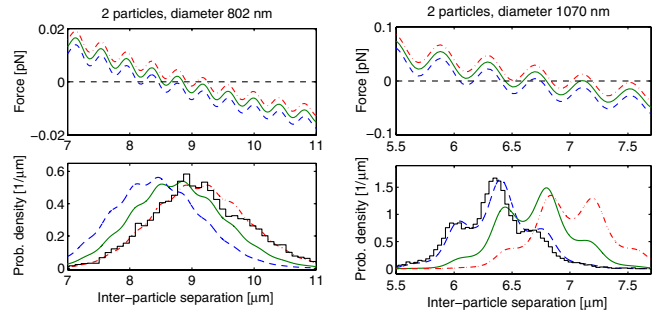

FIG. 3 (color online).   *Top*: Theoretical dependencies of optical force acting on particle R in a chain of two identical polystyrene spheres of diameters 802 nm (left column) and 1070 nm (right column). The equilibrium positions are localized at the separations with zero total force and negative slope (indicating a stable equilibria with the nearest separations between them close to λ_w). *Bottom:* Plots of calculated probability densities of interparticle separation enable easier recognition of multistability events separated from each other by $\lambda_\mathrm{w} = 409$ nm and also comparison with experimental results (see the stairlike black curves). The same parameters as in Fig. 1 were used for calculations except the Bessel beam core radii $\rho_0 = 1.77$ μm (blue dashed), $\rho_0 = 1.80$ μm (green full) and $\rho_0 = 1.83 \mu$m (red dash-dot).

optical forces acting upon sphere R and also the probability density of finding objects with given IPS. For the BB cores we consider, larger particles (diameter 1070 nm) are bound more tightly and create a stable chain with mean IPS ranging from 6 to 7 μm.

However, three possible stable configurations exist here differing in IPS by about $\lambda_w = 409$ nm and corresponding to three peaks in Fig. 3. Smaller particles move in a much shallower potential energy well with less stable equilibrium positions whose depths are about 10 $\times$ smaller comparing to larger particles. The mean IPS between both particles increases from 8.3 to 9.3 μm with widening of the BB core from 1.77 to 1.83 μm. Because of the weaker binding, smaller particles move farther from the equilibrium position due to the thermal Brownian motion which results in a wider probability density distribution. The plots in Fig. 3 confirm the sensitivity of the IPS to the beam parameters. For example, minuscule variations of beam radius by 30 nm causes shifts of the mean IPS by 0.5 μm. Stairlike curves at the bottom of Fig. 3 represent the probability densities of IPS for two optically bound identical polystyrene spheres obtained from 17 000 and 19 300 positions measurements for sphere diameters 802 nm and 1070 nm, respectively.

The probability distribution shape fits well to the CDM model if we assume the BBs core radii is 1.77 μm. For smaller particles (802 nm) we obtained the best fit for BBs core radii 1.83 μm. Positions and shapes coincide very well with the CDM numerical predictions considering the sensitivity of ISP to the BB core radii and the measured spread of the BB core radii in the range 1.79–1.83 μm. The separation between peaks also verifies that the origin of this phenomenon comes from the interference of CP incident and scattered waves as described in Fig. 2 within the used simplification.

Short-range multistability of chain with more particles.—To date few experimental results are available for the longitudinal optical binding of large numbers of objects [3,4,21,22] and no systematic treatment is available, for example, with respect to the object sizes. Quantitative theoretical and experimental analyses are usually restricted only to the behavior of two particles because of the complexity and sensitivity of longitudinal optical binding to experimental parameters [18]. We focused on the comparison of experimentally obtained self-arrangement of multiple identical objects with theoretical predictions using the same setup, objects and procedures described above. An increase in the number of particles in a chain leads to reduction of IPS (see Fig. 4). If, however, a single stable chain is formed from four or more particles, the IPS are no longer equidistant and differ according to the position of the particles with respect to the chain center. In general the IPS is smaller if both particles are placed closer to the chain center. In order to make the numerical study feasible for more particles in the chain we assumed—in agreement with the experiments—that the IPS are the same for particles placed symmetrically with respect to the chain center.
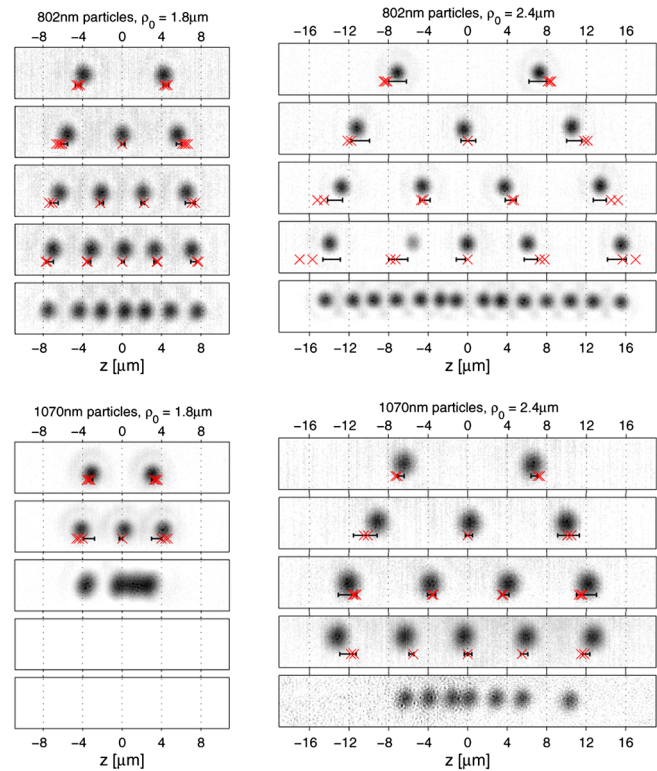

FIG. 4 (color online). Short-range self-arrangement of multiple identical polystyrene particles in a single chain. Left and right column corresponds to Bessel beam core radii $\rho_0 = 1.8$ μm and $\rho_0 = 2.4$ μm, respectively. The upper (lower) row of pictures shows particles of 802 nm (1070 nm) in diameter. The black spots in the individual pictures represent the snapshots of a single particle (mean background intensity subtracted for each image). The horizontal black bar shows the standard deviation of particle positions. The red $\times$ denote the calculated position of the particle center (the same parameters used as in Fig. 3), clusters of $\times$ indicate the short-range multistability events for the cases we could theoretically model.

The results are summarized in Fig. 4 which illustrates that the experimentally obtained positions fit very well with the calculated ones by CDM. The measured probability densities of IPS for configurations from Fig. 4 have clearly distinguished peaks that prove the particles jumps between neighboring equilibrium positions (data not shown). Analogous to the case of two particles, the jumps were more pronounced for 1070 nm particles.

Limiting number of particles in a chain.—Another new phenomenon we observed is the existence of maximal number of bound particles for which the bound chain is stable with well separated particles. Exceeding this number leads to a "phase transition" towards a close-packed configuration with particles almost in physical contact. However this configuration is unstable along the BB axis and is rapidly removed from the original chain position. Particles of diameter 1070 nm placed into the narrower and wider beams do not form chain with more than 3 and 5 particles, respectively. This behavior is supported by the CDM model. Smaller particles (802 nm in diameter),
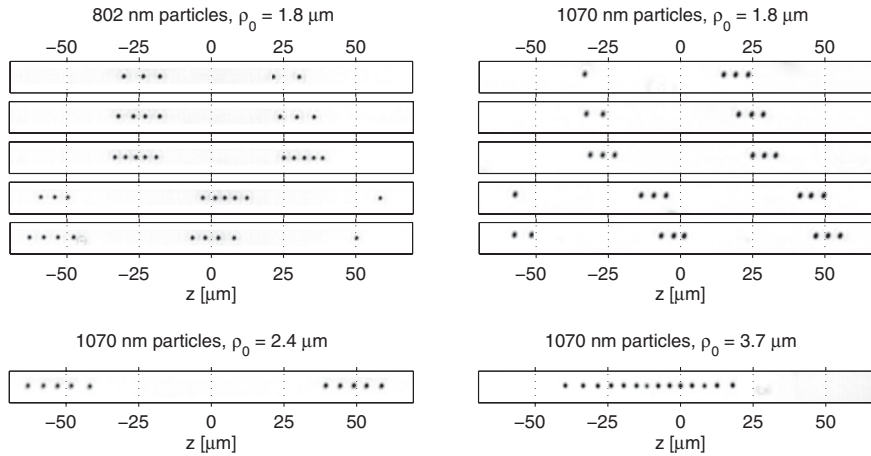
FIG. 5.   *Top:* Formation of chains with more particles of diameter 802 nm (left) or 1070 nm (right). *Bottom:* Self-arrangement of 1070 nm particles in wider BB cores of radii $\rho_0 = 2.4$ μm and $\rho_0 = 3.7$ μm.

however, form chains with more particles, up to 7 in a narrower BB and up to 14 in a wider beam (see Fig. 4). There exists a rapid decrease of IPS for these configurations.

Long-range multistability: Formation of more chains.— As explained in Figs. 1 and 2 long-range equilibrium positions are mainly created as the result of interference of forward-scattered field with the incident BB. For tiny (Rayleigh) particles this part of the total binding force is negligible [23] but in our experiments with submicrometer and micrometer sized spheres many stable chains exist (see Fig. 5) and they form a self-organized one-dimensional structure over maximal observed range of 200 μm. The observed distances between the centers of the chains correspond well with the analytical approximation to the length of the waves ($\lambda_W = 50$ and 90 μm for BB core size 1.8 and 2.4 μm). Therefore the use of wider BB cores provides larger separation between chains and also ensures that more objects are organized within a single chain. This leads to long-range one-dimensional self-organized structures of micrometer and submicrometer objects and represents a step towards the generation of large-scale self-assembled optically bound matter.

Conclusion.—We explained how microparticles placed into two counterpropagating incoherent Bessel beams create extended bound particle chains exhibiting short and long-range multistability.

---

*zemanek@isibrno.cz
URL: www.isibrno.cz/omitec

[1] M. M. Burns, J.-M. Fournier, and J. A. Golovchenko, Phys. Rev. Lett. **63**, 1233 (1989).
[2] M. M. Burns, J.-M. Fournier, and J. A. Golovchenko, Science **249**, 749 (1990).
[3] S. A. Tatarkova, A. E. Carruthers, and K. Dholakia, Phys. Rev. Lett. **89**, 283901 (2002).
[4] W. Singer *et al.*, J. Opt. Soc. Am. B **20**, 1568 (2003).
[5] V. Garcés-Chávez *et al.*, Appl. Phys. Lett. **85**, 4001 (2004).
[6] T. Čižmár *et al.*, Appl. Phys. Lett. **86**, 174101 (2005).
[7] T. Čižmár, M. Šiler, and P. Zemánek, Appl. Phys. B **84**, 197 (2006).
[8] We used a similar setup as in Ref. [7] but a low coherence fiber laser (IPG ILM-10-1070-LP) was employed to suppress interference between the counterpropagating beams. Two identical paths contained conical lenses EKSPLA 130-0270 and demagnifying telescopes composed of lenses Thorlabs LA1433-B ($f = 150$ mm) and three sets of doublets ($f_D = 30, 40, 60$ mm) giving the following measured Bessel beam radii [9] for the beam coming from the left (ρ_{0L}) and right (ρ_{0R}): $\rho_{0L} = 1.787 \pm 0.002$ μm and $\rho_{0R} = 1.827 \pm 0.002$ μm for $f_D = 30$ mm; $\rho_{0L} = 2.44 \pm 0.01$ μm and $\rho_{0R} = 2.43 \pm 0.05$ μm for $f_D = 40$ mm, and $\rho_{0L} = 3.75 \pm 0.01$ μm and $\rho_{0R} = 3.70 \pm 0.02$ μm for $f_D = 60$ mm. Tracing the beam through the optical setup gave an estimate of the on-axis optical intensity as 4 mW/μm^2.
[9] T. Čižmár *et al.*, New J. Phys. **8**, 43 (2006).
[10] E. M. Purcell and C. R. Pennypacker, Astrophys. J. **186**, 705 (1973).
[11] B. Draine, Astrophys. J. **333**, 848 (1988).
[12] P. C. Chaumet and M. Nieto-Vesperinas, Phys. Rev. B **61**, 14119 (2000).
[13] V. Karásek, K. Dholakia, and P. Zemánek, Appl. Phys. B **84**, 149 (2006).
[14] A. G. Hoekstra *et al.*, J. Opt. Soc. Am. A **18**, 1944 (2001).
[15] F. Depasse and J. M. Vigoureux, J. Phys. D **27**, 914 (1994).
[16] T. M. Grzegorczyk, B. A. Kemp, and J. A. Kong, Phys. Rev. Lett. **96**, 113903 (2006).
[17] J. Ng *et al.*, Phys. Rev. B **72**, 085130 (2005).
[18] N. K. Metzger, K. Dholakia, and E. M. Wright, Phys. Rev. Lett. **96**, 068102 (2006).
[19] N. K. Metzger, E. M. Wright, and K. Dholakia, New J. Phys. **8**, 139 (2006).
[20] V. Karásek, T. Čižmár, and P. Zemánek, in *Optical Trapping and Optical Micromanipulation III: Proceedings of SPIE*, edited by K. Dholakia and G. C. Spalding (2006), Vol. 6326, p. 632608.
[21] N. K. Metzger *et al.*, Opt. Express **14**, 3677 (2006).
[22] D. M. Gherardi *et al.*, Appl. Phys. Lett. **93**, 041110 (2008).
[23] V. Karásek and P. Zemánek, J. Opt. A Pure Appl. Opt. **9**, S215 (2007).